Biomedical Optics EXPRESS

Tensor total variation approach to optical coherence tomography reconstruction for improved visualization of retinal microvasculature

Alexander Wong,[1,*] **Sepideh Hariri,**[2] **Eun Sun Song,**[2] **and Kostadinka Bizheva**[2]

[1]*Dept. of Systems Design Engineering, University of Waterloo, Waterloo, ON N2L3G1, Canada*

[2]*Dept. of Physics and Astronomy University of Waterloo, Waterloo, ON N2L3G1, Canada*

**a28wong@uwaterloo.ca*

Abstract:
A novel optical coherence tomography (OCT) reconstruction approach is introduced for improved visualization of inner-retina capillaries in retinal OCT tomograms. The proposed method utilizes a minimization framework based on a tensor total variation (TTV) energy functional, to enforce capillary structural characteristics in the spatial domain. By accounting for structure tensor characteristics, the TTV reconstruction method allows for contrast enhancement of capillary structural characteristics. The novel TTV method was tested on high resolution OCT images acquired *in-vivo* from the foveal region of the retina of a healthy human subject. Experimental results demonstrate significant contrast and visibility enhancement of the inner retina capillaries in the retinal OCT tomograms, achieved by use of the TTV reconstruction method. Therefore, the TTV method has a strong potential for improved disease progression analysis based on the study of disease-induced changes in the inner retina vasculature.

OCIS codes: (170.4500) Optical coherence tomography; (100.0100) Image processing; (100.2980) Image enhancement; (100.3008) Image recognition, algorithms and filters.

References and links

1. E. Friedman, "A hemodynamic model of the pathogenesis of age-related macular degeneration," Am. J. Ophthalmol. **124**, 677–682 (1997).
2. J. Flammer, S. Orgül, V. P. Costa, N. Orzalesi, G. K. Krieglstein, L. M. Serra, J.-P. Renard, and E. Stefansson, "The impact of ocular blood flow in glaucoma," Prog. Retin. Eye Res. **21**, 359–393 (2002).
3. V. Patel, S. Rassam, R. Newsom, J. Wiek, and E. Kohner, "Retinal blood flow in diabetic retinopathy," Br. Med. J. **305**(6855), 678–683 (1992).
4. S. Dithmar, and F. G. Holz, *Fluorescence Angiography in Ophthalmology* (Springer, 2008).
5. M. Hope-Ross, L. A. Yannuzzi, E. S. Gragoudas, D. R. Guyer, J. S. Slakter, J. A. Sorenson, S. Krupsky, D. A. Orlock, and C. A. Puliafito, "Adverse reactions due to indocyanine green," Ophthalmology **101**, 529–533 (1994).
6. L. A. Yannuzzi, K. T. Rohrer, L. J. Tindel, R. S. Sobel, M. A. Costanza, W. Shields, and E. Zang, "Fluorescein angiography complication survey," Ophthalmology **93**, 611–617 (1986).
7. C. E. Riva, G. T. Feke, B. Eberli, and V. Benary, "Bidirectional LDV system for absolute measurement of blood speed in retinal vessels," Appl. Opt. **18**, 2301–2306 (1979).
8. G. Michelson, B. Schmauss, M. Langhans, J. Haraznv, and M. Groh, "Principle, validity, and reliability of scanning laser Doppler flowmetry," J. Glaucoma **5**, 99–105 (1996).

#156422 - $15.00 USD Received 12 Oct 2011; revised 29 Nov 2011; accepted 29 Nov 2011; published 19 Dec 2011

9. Y. Tamaki, M. Araie, E. Kawamoto, S. Eguchi, and H. Fujii, "Noncontact, two-dimensional measurement of retinal microcirculation using laser speckle phenomenon," Invest. Ophthalmol. Vis. Sci. **35**, 3825–3834 (1994).
10. D. Huang, E. A. Swanson, C. P. Lin, J. S. Schuman, W. G. Stinson, W. Chang, M. R. Hee, T. Flotte, K. Gregory, C. A. Puliafito, and J. G. Fujimoto, "Optical coherence tomography," Science **254**, 1178–1181 (1991).
11. A. F. Fercher, "Optical coherence tomography," J. Biomed. Opt. **1**, 157–173 (1996).
12. X. J. Wang, T. E. Milner, and J. S. Nelson, "Characterization of fluid flow velocity by optical Doppler tomography," Opt. Lett. **20**(11), 1337–1339 (1995).
13. Y. Zhao, Z. Chen, C. Saxer, S. Xiang, J. F. de Boer, and J. S. Nelson, "Phase-resolved optical coherence tomography and optical Doppler tomography for imaging blood flow in human skin with fast scanning speed and high velocity sensitivity," Opt. Lett. **25**(2), 114–116 (2000).
14. R. Leitgeb, L. Schmetterer, W. Drexler, A. Fercher, R. Zawadzki, and T. Bajraszewski, "Real-time assessment of retinal blood flow with ultrafast acquisition by color Doppler Fourier domain optical coherence tomography," Opt. Express **11**(23), 3116–3121 (2003).
15. M. Szkulmowski, A. Szkulmowska, T. Bajraszewski, A. Kowalczyk, and M. Wojtkowski, "Flow velocity estimation using joint spectral and time domain optical coherence tomography," Opt. Express **16**(9), 6008–6025 (2008).
16. Y. K. Tao, A. M. Davis, and J. A. Izatt, "Single-pass volumetric bidirectional blood flow imaging spectral domain optical coherence tomography using a modified Hilbert transform," Opt. Express **16**(16), 12350–12361 (2008).
17. A. H. Bachmann, M. L. Villiger, C. Blatter, T. Lasser, and R. A. Leitgeb, "Resonant Doppler flow imaging and optical vivisection of retinal blood vessels," Opt. Express **15**(2), 408-422 (2007).
18. R. K. Wang, S. L. Jacques, Z. Ma, S. Hurst, S. R. Hanson, and A. Gruber, "Three dimensional optical angiography," Opt. Express **15**(7), 4083–4097 (2007).
19. H. Ren, Y. Wang, J. Stuart Nelson, and Z. Chen, "Power optical Doppler tomography imaging of blood vessel in human skin and M-mode Doppler imaging of blood flow in chick chorioallantoic membrane," Proc. SPIE **4956** 225–231 (2003).
20. H. Ren, T. Sun, D. J. MacDonald, M. J. Cobb, and X. Li, "Real time in vivo blood-flow imaging by moving-scatterer-sensitive spectral-domain optical Doppler tomography," Opt. Lett. **31** 927–929 (2006).
21. H. Ren and X. Li, "Clutter rejection filters for optical Doppler tomography," Opt. Express **14** 6103–6112 (2006).
22. T. Schmoll, C. Kolbitsch, and R. A. Leitgeb, "Ultra-high-speed volumetric tomography of human retinal blood flow," Opt. Express **17**(5), 4166–4176 (2009).
23. S. Makita, T. Fabritius, and Y. Yasuno, "Quantitative retinal-blood flow measurement with three-dimensional vessel geometry determination using ultrahigh-resolution Doppler optical coherence angiography," Opt. Lett. **33**(8), 836–838 (2008).
24. A. Szkulmowska, M. Szkulmowski, D. Szlag, A. Kowalczyk, and M. Wojtkowski, "Three-dimensional quantitative imaging of retinal and choroidal blood flow velocity using joint Spectral and Time domain Optical Coherence Tomography," Opt. Express **17**(13), 10584–10598 (2009).
25. T. N. Crawford, D. V. Alfaro 3rd, J. B. Kerrison, and E. P. Jablon, "Diabetic retinopathy and angiogenesis," Curr. Diabetes Rev. **5**(1), 8–13 (2009).
26. H. Kokotas, M. Grigoriadou, and M. B. Petersen, "Age-related macular degeneration: genetic and clinical findings," Clin. Chem. Lab. Med. **49**(4), 601–616 (2011).
27. L. An, and R. K. Wang, "In vivo volumetric imaging of vascular perfusion within human retina and choroids with optical micro-angiography," Opt. Express **16**(15), 11438–11452 (2008).
28. J. Fingler, R. J. Zawadzki, J. S. Werner, D. Schwartz, and S. E. Fraser, "Volumetric microvascular imaging of human retina using optical coherence tomography with a novel motion contrast technique," Opt. Express **17**(24), 22190–22200 (2010).
29. Z. Zhi, W. Cepurna, E. Johnson, T. Shen, J. Morrison and R. K. Wang, "Volumetric and quantitative imaging of retinal blood flow in rats with optical microangiography," Biomed. Opt. Express **2**(3), 579–591 (2011).
30. S. Makita, F. Jaillon, M. Yamanari, M Muira and Y. Yasuno, "Comprehensive in vivo micro-vascular imaging of the human eye by dual-beam-scan Doppler optical coherence angiography," Opt. Express **19**(2), 1271–1283 (2011).
31. S. Zotter, M. Pirchser, T Torzicky, M. Bonesi, E. Geotzinger, R. Leitgeb and C. Hitzenberger, "Visualization of microvasculature by dual-beam phase-resolved Doppler optical coherence tomography," Opt. Express **19**(2), 1217–1227 (2011).
32. R. A. Leitgeb, T. Schmoll, A. S. G. Singh, E. Diettrich, and G. Langs, "Comprehensive OCT imaging of retinal microvasculature without adaptive optics", presented at Photonics West (BIOS), San Francisco, California, USA, January 22–27, 2011.
33. P. Puvanathasan, P. Forbes, Z. Ren, D. Malchow, S. Boyd and K. Bizheva, "High-speed, high-resolution Fourier-domain optical coherence tomography system for retinal imaging in the 1060 nm wavelength region," Opt. Lett. **33**, 2479–2481 (2008).
34. S. Hariri, A. A. Moayed, A. Dracopolos, C. Hyun, S. Boyd and K. Bizheva, "Limiting factors to the OCT axial resolution for in-vivo imaging of human and rodent retina in the 1060nm wavelength range," Opt. Express **17**(26) 24304–24316 (2009).

#156422 - $15.00 USD Received 12 Oct 2011; revised 29 Nov 2011; accepted 29 Nov 2011; published 19 Dec 2011

35. A. Mishra, A. Wong, K. Bizheva and D. A. Clausi, "Interactive approach to intraretinal layer segmentation in optical coherence tomography images," Opt. Express **17**(26) 23719–23728 (2009).
36. D. Cabrera Fernández, H. M. Salinas, and C. A. Puliafito, "Automated detection of retinal layer structures on optical coherence tomography images," Opt. Express **13** 10200–10216 (2005).
37. P. Perona and J. Malik, "Scale-space and edge detection using anisotropic diffusion," IEEE Trans. Pattern Anal. Mach. Intell. **12** 629–639 (1990).
38. G. H. Cottet and L. Germain, "Image processing through reaction combined with nonlinear diffusion," Math. Comp. **61** 659–673 (1993).
39. J. Weickert, "Foundations and applications of nonlinear anisotropic diffusion filtering," Z. Angew. Math. Mech. **76**(1) 283–286 (1996).
40. J. Weickert, "Coherence-enhancing diffusion filtering," Int. J. Comput. Vision **31** 111–127 (1999).
41. A. Roussos and P. Maragos, "Tensor-based image diffusions derived from generalizations of the Total Variation and Beltrami Functionals," in *2010 17th IEEE International Conference on Image Processing (ICIP)* (2010), pp. 4141–4144 .
42. M. Fedoryuk, "Method of steepest descent," *Encyclopaedia of Mathematics* (Springer, 2001).
43. R. Nowak, "Wavelet-based Rician noise removal for magnetic resonance imaging," IEEE Trans. Image Process. **8**(10), 1408–1419 (1999).

1. Introduction

Potentially blinding retinal diseases such as age-related macular degeneration [1] (AMD), glaucoma [2] and diabetic retinopathy [3] cause significant changes in the retinal and choroidal vasculature and blood flow. Currently, standard clinical practice relies on fluorescent angiography [4] (FA) and indocyanine green angiography [5] (ICGA) for assessment of impaired retinal and choroidal blood flow respectively, in retinal pathologies. Since both FA and ICGA require intravenous injection of contrast agents, these methods are considered invasive and have been shown to be associated with various negative side effects in a subset of patients [5, 6].

Non-invasive optical methods such as laser Doppler velocimetry (LDV) [7], scanning laser Doppler flowmetry [8], laser speckle flowgraphy [9] have been utilized in the past for imaging retinal perfusion and measurement of the red blood cells average velocity and total blood flow in retinal and choroidal vessels. Since all of these methods are based on highly coherent light detection, they have a common shortcoming: poor discrimination between blood vessels located at different depths inside the retina or choroid.

Optical coherence tomography (OCT) is a non-invasive imaging modality based on detection of partially coherent light. As such, this technique allows for depth-resolved, cellular level resolution imaging of the structural composition of biological tissue at depths up to 1-2mm in scattering tissue [10, 11]. The ability of OCT to measure both the intensity and the phase of the scattered light has been utilized for development of Doppler OCT (D-OCT) for imaging and quantification of blood flow [12]. Since 1995, various D-OCT system designs, data acquisition schemes and data processing algorithms have been proposed for measuring the blood flow and mapping the vasculature of biological tissue [13–21]. Different versions of the D-OCT technology have been successfully used for mapping the perfusion of the human retina and choroid and for precise measurement of retinal and choroidal blood flow [22–24, 27–31].

Since retinal diseases such as AMD and diabetic retinopathy have been shown to alter the capillary networks in the inner and outer plexiform layers of the retina [25, 26], precise mapping of the inner retina microvasculature throughout different stages of the disease development may prove a useful marker for early disease diagnostics and evaluation of the efficacy of drug and surgical therapeutic approaches. Visualization of the inner retina capillaries on intensity based structural 3D OCT tomograms of the human retina is not optimal due to their fairly low optical contrast. The use of D-OCT technologies such as optical microangiography [27] (OMAG), motion contrast OCT [28], dual-beam phase-resolved D-OCT [31] and dual-beam-scan D-OCT [30], has been proven to improve the contrast and visibility of the inner retina microvasculature. However, all of these methods require complicated hardware, data and im-

#156422 - $15.00 USD Received 12 Oct 2011; revised 29 Nov 2011; accepted 29 Nov 2011; published 19 Dec 2011

age processing software and/or time-consuming data acquisition procedures. An alternative approach would be to develop and utilize image processing algorithms that can be applied to structural OCT images of the retina for improved visualization of the retinal microvasculature. Preliminary results from such approaches, based on filtering techniques and random forest classification techniques were recently announced [32].

Here we present a novel OCT reconstruction method designed particularly to enhance the visualization of the capillary networks in the inner retina in structural retinal OCT tomograms. The novelty of the algorithm stems from the addition of a minimization framework used to reconstruct spatial domain data based on a tensor total variation (TTV) energy functional. This allows the reconstruction method to emphasize and enforce structural characteristics in a dynamic fashion to significantly enhance the visibility of coherent image features such as inner retina capillaries, even in the presence of speckle noise.

2. Methods

In the proposed framework for improving the visualization of inner retina microvasculature in human retina OCT tomograms, the human retina was imaged *in-vivo* with a research grade high speed, ultrahigh resolution (UHROCT) system operating in the 1060nm wavelength region. The basic design and detailed description of the system was published [33] previously, however, the light source and the camera were recently updated to improve the axial resolution in the human retina and the image acquisition rate. Briefly, the UHROCT system used in this study is based on a spectral domain design, that utilizes a fiber-based Michelson interferometer interfaced to a super-luminescent diode (Superlum, λc = 1020nm, $\delta\lambda$ = 110nm, P_{out} = 10mW). The spectral output of the light source was custom designed to include a high power peak at $\sim$980nm where water absorption has a local maximum. As demonstrated with a computational model [34], the use of such spectral shaping can result in an improved axial resolution in the retina during *in-vivo* imaging. In this study, the use of the custom light source resulted in $\sim 5\mu$m axial and $\sim 15\mu$m lateral resolution in retinal tissue. Retinal tomograms were acquired with a novel InGaAs linear array, 1024 pixel camera (SUI, Goodrich) with 92kHz readout rate, that was interfaced with a high performance spectrometer (P&P Optica). The UHROCT system provided 95dB SNR for 1.3mW optical power incident on the human retina.

Volumetric images (512 x 512 x 512, corresponding to $\sim 10^o$ scanning angle) were acquired *in-vivo* and reconstructed using the proposed TTV reconstruction method from the foveal region of the retina of a human subject. The imaging procedure was carried out in accordance with the University of Waterloo ethics regulations. Next, the tomograms were segmented at the retinal pigmented epithelium (RPE), using an automatic segmentation algorithm [35] and flattened by shifting adjacent A-scans to straighten the RPE layer. Subsequently, the stack of flattened retinal images was rendered in 3D and a sub-volume was obtained from locations corresponding to the interface between the inner plexiform and inner nuclear layers, and the outer plexiform layer of the retina, to visualize the inner retina microvasculature. The methodology behind the proposed TTV reconstruction method is described in detail in the subsequent section.

2.1. Proposed TTV reconstruction

In OCT, a broad bandwidth light source is used to illuminate the imaged object at location (x,y). The back-scattered light from the object interferes with a reference optical beam with known optical delay. The intensity of the interference signal $S(z)$, measured at a location (x,y), is a function of depth z in the imaged object. In traditional reconstruction methods, a 3D volumetric image $S(x,y,z)$ is constructed by directly combining the axial scans $S(z)$ acquired at different locations (x,y). However, such a traditional volumetric reconstruction, when applied to 3D OCT images of the human retina, results is fairly poor contrast of structural features

#156422 - $15.00 USD Received 12 Oct 2011; revised 29 Nov 2011; accepted 29 Nov 2011; published 19 Dec 2011

such as the microvasculature of the inner retina. The presence of speckle noise in retinal OCT images hinders the visualization and analysis of small structural details such as retinal capillaries. Fortunately, retinal capillaries have strong, distinctive structural characteristics when compared with the surrounding tissue. Therefore, an enhanced reconstruction mechanism that emphasizes and enforces structural characteristics within the underlying data, could improve the visualization of the inner retina microvasculature.

Here, we propose the concept of tensor total variation reconstruction, where a minimization framework is developed and incorporated into the data reconstruction process based on a tensor total variation energy functional, a functional that is inspired by nonlinear diffusion strategies [36–40], and can be described as follows.

2.1.1. Three-dimensional structure tensor

For simplification, let $\underline{x}$ denote a vector representing the spatial coordinates (x,y,z). Let $S(\underline{x})$ represent the 3D volumetric image. The structure tensor $J(\nabla S)$ characterizes the geometry of local structures within S and can be defined as a symmetric positive definite matrix expressed by

$$J(\nabla S) = K(\sigma) * (\nabla S \cdot \nabla S^T), \tag{1}$$

where $K(\sigma)$ is a Gaussian kernel with a spread defined by σ, $*$ is the convolution operator, and $\cdot$ is the dot product operator. The eigen-decomposition of $J(\nabla S)$ can be expressed by

$$J(\nabla S) = [\phi_1 \;\; \phi_2 \;\; \phi_3] \begin{bmatrix} \lambda_1 & 0 & 0 \\ 0 & \lambda_2 & 0 \\ 0 & 0 & \lambda_3 \end{bmatrix} [\phi_1 \;\; \phi_2 \;\; \phi_3]^T, \tag{2}$$

where the eigenvectors ϕ_1, ϕ_2, and ϕ_3 define the local structure orientation, while the eigenvalues λ_1, λ_2, and λ_3 define the signal change according to the orientation defined by the eigenvectors. A 3D hyperellipsoid visualization of the structure tensor is shown in Fig. 1.

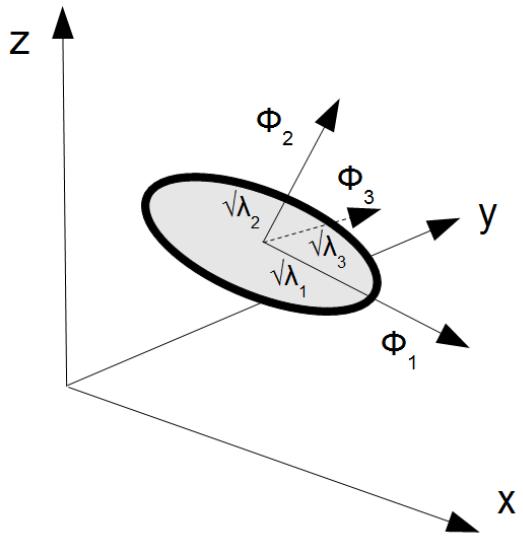

Fig. 1. A 3D hyperellipsoid visualization of the structure tensor.

#156422 - $15.00 USD Received 12 Oct 2011; revised 29 Nov 2011; accepted 29 Nov 2011; published 19 Dec 2011

2.1.2. Tensor total variation minimization

Given the structure tensor $J(\nabla S)$, extending upon the seminal work by Roussos and Maragos on the tensor functionals [41], the tensor energy functional used in TTV reconstruction for enforcing structural characteristics within the underlying data S can be defined as

$$E(S) = \int_{\Omega} \left[\sqrt{\lambda_1(J(\nabla S))} + \sqrt{\lambda_2(J(\nabla S))} + \sqrt{\lambda_3(J(\nabla S))} \right] d\underline{x}, \tag{3}$$

where Ω defines the image domain. Therefore, based on this tensor energy functional $E(S)$, the TTV reconstructed 3D volumetric image S_c can be defined as the 3D volumetric image configuration that minimizes $E(S)$,

$$S_c = \arg\min_{S} \int_{\Omega} \left[\sqrt{\lambda_1(J(\nabla S))} + \sqrt{\lambda_2(J(\nabla S))} + \sqrt{\lambda_3(J(\nabla S))} \right] d\underline{x}. \tag{4}$$

In practice, the TTV reconstructed 3D volumetric image S_c can be computed via a steepest descent optimization strategy [42], where the steepest descent for minimizing the tensor energy functional $E(s)$ can be expressed as

$$\frac{\partial S}{\partial t} = div\left(K(\sigma) * \left(\frac{1}{\sqrt{\lambda_1}} \phi_1 \cdot \phi_1^T + \frac{1}{\sqrt{\lambda_2}} \phi_2 \cdot \phi_2^T + \frac{1}{\sqrt{\lambda_3}} \phi_3 \cdot \phi_3^T \right) \nabla S \right). \tag{5}$$

As such, if we were to let the initial state be the set of directly combined axial scans $S_c^{\,0} = S$, the TTV reconstructed 3D volumetric image S_c at iteration $t+1$ of the optimization process can be written as

$$S_c^{\,t+1} = S_c^{\,t} + q\Delta S^{\,t}, \tag{6}$$

where $\Delta S^{\,t}$ is the discretization of $\frac{\partial S}{\partial t}$ in Eq. 5, and q controls the degree of descent. We found that the use of the directly combined axial scans $S_c^{\,0} = S$ as the initial solution to provide sufficiently fast convergence (approximately 15 iterations based on empirical testing with human retinal data sets acquired *in-vivo*). Furthermore, using the directly combined axial scans acts as a good initial solution given that it allowed for convergence to the global minima for our test cases. One consideration to take into account is that for situations where the signal-to-noise ratio of the acquired data is much lower than the data presented here, the convergence rate would increase as the initial solution would be farther from the desired solution, and hence require greater number of iterations to reach the desired solution.

3. Results and discussion

To test the effectiveness of the proposed TTV reconstruction method for improving the visualization of inner retina microvasculature in human retina OCT tomograms, the method was applied on a human retinal data set acquired *in-vivo*. The data set was processed with the novel TTV reconstruction method using the steepest descent optimization strategy described in Eq. 6. A total of 15 iterations was performed as it was found to provide strong reconstruction performance, with $q = 1$ in Eq. 6, and $\sigma = 1$ for kernel K. Processing time was $\sim$50 sec for each sub-volume on an Intel Core 2 Duo 1.67 GHz PC with 2 GB of RAM. Fig. 2 shows en-face projections from the 3D UHROCT retinal tomogram.

The image in Fig. 2 shows the retinal capillary network with fairly low contrast, with a central a-vascular region at the location of the fovea. Note that the capillaries located at the edges of the a-vascular area are poorly visible. The image in fig. 2C shows a projection in depth of the outer nuclear and photoreceptor layers up to the outer limiting membrane. Note that the capillaries surrounding the a-vascular foveal region appear of higher contrast than similar vessels at larger

#156422 - $15.00 USD Received 12 Oct 2011; revised 29 Nov 2011; accepted 29 Nov 2011; published 19 Dec 2011

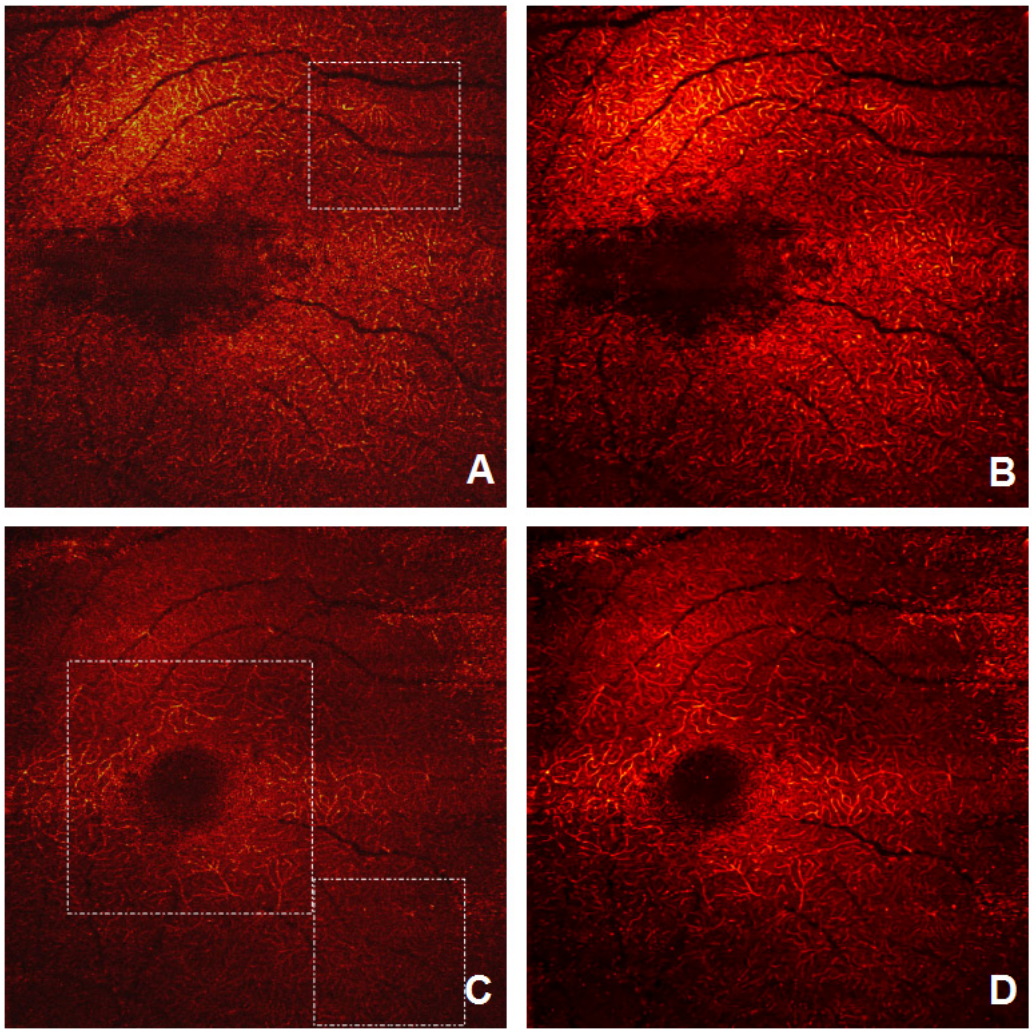

Fig. 2. En-face projections from 3D volume showing retinal microvasculature. Same en-face projections processed with the novel TTV reconstruction method with $q = 1$ (B and D). White dashed-line squares in A and C mark areas of interest that were magnified and displayed in Fig. 3.

radial distances from the foveal center. This effect is most likely due to the difference in the natural curvatures of the outer plexiform layer and the RPE close to the foveal center.

The corresponding en-face projections from the sub-volume reconstructed using the TTV reconstruction method are shown in Fig. 2B and Fig. 2D. The overall visibility of the retinal capillaries was improved, specifically at the rim of the a-vascular area.

A total of three areas of interests were marked in the projections of the standard reconstructed volume (Fig. 2A and Fig. 2C) with a white dashed-line squares, provide a closer look at the improvement of the visibility of certain imaging features. The magnified images are presented in Fig. 3. A magnification factor of 3x was used for Fig. 3(A-B) and Fig. 3(E-F), while a magnification factor of 2x was used for Fig. 3(C-D). En-face projections from the sub-volume reconstructed using the novel TTV reconstruction method are shown in Fig. 3B, Fig. 3D, and

#156422 - $15.00 USD Received 12 Oct 2011; revised 29 Nov 2011; accepted 29 Nov 2011; published 19 Dec 2011

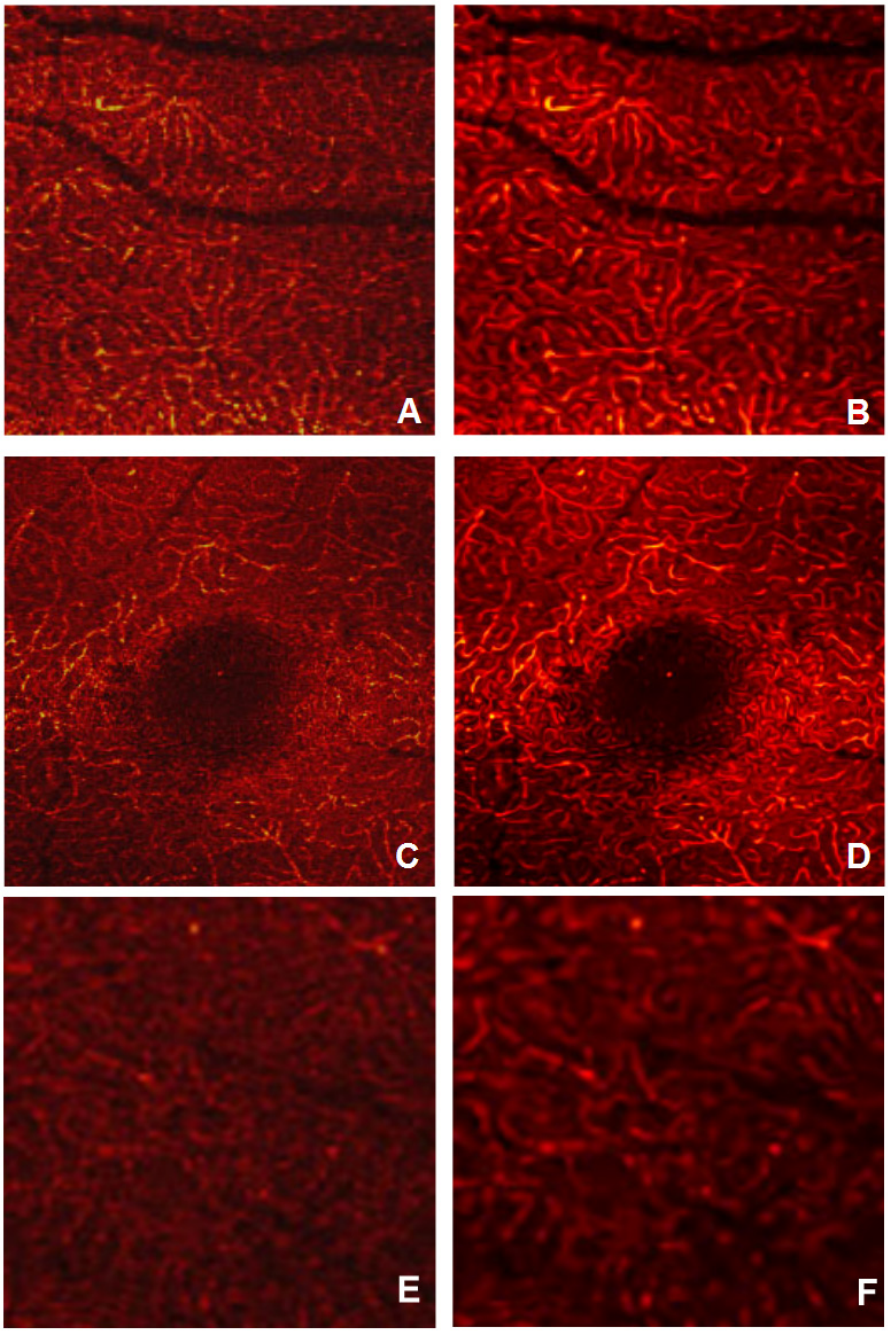

Fig. 3. Magnified view of the areas of interest marked with the white dashed-line squares in Fig. 2A and Fig. 2C. A magnification factor of 3x was used for (A-B) and (E-F), while a magnification factor of 2x was used for (C-D). En-face projections from the sub-volume reconstructed using the novel TTV reconstruction method (corresponding to the same white dashed-line squares except for Fig. 2B and Fig. 2D) is shown in (B), (D), and (F).

#156422 - $15.00 USD Received 12 Oct 2011; revised 29 Nov 2011; accepted 29 Nov 2011; published 19 Dec 2011

Fig. 3F. A closer look at Fig. 3 shows that in the case when the contrast of the retinal capillaries in the standard reconstructed volume is fine (Fig. 3A and Fig. 3D), significant improvement of the visibility of the retinal microvasculature without saturation can be obtained using TTV reconstruction (Fig. 3B and Fig. 3D). Furthermore, even in the case when the contrast of the retinal capillaries in the standard reconstructed volume is poor (Fig. 3E), significant improvement of the visibility of the retinal microvasculature without saturation can be obtained using TTV reconstruction (Fig. 3F).

Next, we investigate the effectiveness of TTV reconstruction at improving the contrast between retinal capillaries and surrounding tissue compared to standard reconstruction. This provides us with a good empirical sense as to how well the retinal capillaries can be distinguished, which is important for visual interpretation and analysis. To achieve this goal, the following contrast improvement factor c was measured as [43]

$$c = \left(\frac{E(S^1)+E(S^2)}{E(S^1)-E(S^2)}\right)\left(\frac{E(S_c^1)-E(S_c^2)}{E(S_c^1)+E(S_c^2)}\right), \tag{7}$$

where $E(S^1)$ and $E(S^2)$ are the expected values of the surrounding regions and retinal capillary regions of the standard reconstructed volume S respectively, and $E(S_c^1)$ and $E(S_c^2)$ are the expected values of the surrounding regions and retinal capillary regions of the TTV reconstructed volume S_c respectively. For the tested volumes, it was found that the contrast improvement factor c for TTV reconstruction when compared to standard reconstruction was 2.83. What this indicates is that the contrast between retinal capillaries and surrounding tissue when using TTV reconstruction is significantly improved over standard reconstruction, when is very important for improving the visualization of retinal microvasculature.

In terms of improving the visualization of inner retinal microvasculature in retinal UHROCT tomograms, the proposed novel TTV reconstruction algorithm has some significant advantages over the D-OCT methods mentioned in Section 1 of this paper. For example, the TTV method does not require hardware modifications to the OCT system and can be applied to images acquired with any commercially available or research grade OCT technology. It does not require special scanning protocols that can increase the overall raw imaging data acquisition time or introduce additional motion artifacts. Therefore, this method is not restricted to the specific design of the OCT system and it can be applied to images acquired with any retinal SD-OCT, SS-OCT and TD-OCT, operating at 800nm or 1060nm. Furthermore, the TTV method is not restricted to research grade OCT systems and in principle can be applied to image acquired with any commercial ophthalmic OCT system that can visualize the inner retina microvasculature. In all cases the choice of the initial solution and the number of iterations for convergence may vary, to adapt to the image quality of the retinal data and result in optimal contrast improvement of the imaged microvasculature. Currently, the TTV method has not been tested on OCT images of biological tissue different than human retina. However, we expect that by modifying the input parameters of the algorithm, it can be adapted and optimized for images acquired from different types of biological tissue. The TTV method is fairly fast with the potential of practically real time display of the processed images if combined with FPGA or CUDA technology. In this manuscript, the TTV method was combined with pre-processing stage that involved segmentation and flattening of the retinal tomograms, because we used fairly wide angle images ($\sim 10^o$ scanning angle). This pre-processing step is not a pre-requisite for using the TTV reconstruction method with OCT tomograms and can be omitted, especially in the case when smaller areas of the retina need to be examined.

#156422 - $15.00 USD Received 12 Oct 2011; revised 29 Nov 2011; accepted 29 Nov 2011; published 19 Dec 2011

4. Conclusion

In this paper, we have proposed a novel reconstruction method for retinal UHROCT imagery designed specifically to enhance the visualization of capillary networks in the inner retina. When compared to existing reconstruction methods from research literature using *in-vivo* retinal images, the proposed TTV reconstruction demonstrates superior contrast and visibility of the underlying capillary network structure, even in the presence of speckle noise. When combined with segmentation algorithms designed for blood vessels, the proposed algorithm can result in improved precision of the quantitative measurement of the blood vessel diameter, a parameter that is needed for quantitative investigation of blood flow.

Acknowledgments

This work was supported in part by the Natural Sciences and Engineering Research Council of Canada (NSERC) and the University of Waterloo research grants.

#156422 - $15.00 USD Received 12 Oct 2011; revised 29 Nov 2011; accepted 29 Nov 2011; published 19 Dec 2011